Investigation of hillslope vineyard soil water dynamics using field measurements and numerical modeling

Krevh, Vedran; Groh, Jannis; Weihermüller, Lutz; Filipović, Lana; Defterdarović, Jasmina; Kovač, Zoran; Magdić, Ivan; Lazarević, Boris; Baumgartl, Thomas; Filipović, Vilim

Article

Investigation of Hillslope Vineyard Soil Water Dynamics Using Field Measurements and Numerical Modeling

Vedran Krevh [1,*], Jannis Groh [2,3,4], Lutz Weihermüller [3], Lana Filipović [1], Jasmina Defterdarović [1], Zoran Kovač [5], Ivan Magdić [6], Boris Lazarević [7], Thomas Baumgartl [8] and Vilim Filipović [1,8]

1   Department of Soil Amelioration, Faculty of Agriculture, University of Zagreb, 10000 Zagreb, Croatia
2   Institute of Crop Science and Resource Conservation—Soil Science and Soil Ecology, University of Bonn, 53113 Bonn, Germany
3   Institute of Bio- and Geoscience (IBG-3, Agrosphere), Forschungszentrum Jülich GmbH, 52428 Jülich, Germany
4   Research Area 1 "Landscape Functioning", Working Group "Hydropedology", Leibniz Centre for Agricultural Landscape Research (ZALF), 5374 Müncheberg, Germany
5   Department of Geology and Geological Engineering, Faculty of Mining Geology and Petroleum Engineering, University of Zagreb, 10000 Zagreb, Croatia
6   Department of Soil Science, Faculty of Agriculture, University of Zagreb, 10000 Zagreb, Croatia
7   Department of Plant Nutrition, Faculty of Agriculture, University of Zagreb, 10000 Zagreb, Croatia
8   Future Regions Research Centre, Geotechnical and Hydrogeological Engineering Research Group, Federation University, Gippsland, VIC 3841, Australia
*   Correspondence: vkrevh@agr.hr

Abstract: Soil heterogeneities can impact hillslope hydropedological processes (e.g., portioning between infiltration and runoff), creating a need for in-depth knowledge of processes governing water dynamics and redistribution. The presented study was conducted at the SUPREHILL Critical Zone Observatory (CZO) (hillslope vineyard) in 2021. A combination of field investigation (soil sampling and monitoring campaign) and numerical modeling with hydrological simulator HYDRUS-1D was used to explore the water dynamics in conjunction with data from a sensor network (soil water content (SWC) and soil-water potential (SWP) sensors), along the hillslope (hilltop, backslope, and footslope). Soil hydraulic properties (SHP) were estimated based on (i) pedotransfer functions (PTFs), (ii) undisturbed soil cores, and (iii) sensor network data, and tested in HYDRUS. Additionally, a model ensemble mean from HYDRUS simulations was calculated with PTFs. The highest agreement of simulated with observed SWC for 40 cm soil depth was found with the combination of laboratory and field data, with the lowest average MAE, RMSE and MAPE (0.02, 0.02, and 5.34%, respectively), and highest average R^2 (0.93), while at 80 cm soil depth, PTF model ensemble performed better (MAE = 0.03, RMSE = 0.03, MAPE = 7.55%, R^2 = 0.81) than other datasets. Field observations indicated that heterogeneity and spatial variability regarding soil parameters were present at the site. Over the hillslope, SWC acted in a heterogeneous manner, which was most pronounced during soil rewetting. Model results suggested that the incorporation of field data expands model performance and that the PTF model ensemble is a feasible option in the absence of laboratory data.

Keywords: numerical modeling; soil-hydraulic properties; pedotransfer functions; hillslope vineyard; soil water content

1. Introduction

Over the last decades, hillslope hydrological research has produced valuable field observations, theories, and models at individual research sites and networks [1–5]. In general, hillslope hydrology is concerned with the redistribution of precipitation and the organization of water availability in the landscape [5] which affects vegetation, soil development, and processes responsible for water and matter flow at the surface and in the subsurface [6]. Since hillslopes are often characterized by a pore system affected by lateral

forces, heterogeneities may result impacting hillslope processes [6], and an insight into the area and its heterogeneity is of uppermost importance to unravel processes governing water dynamics and redistribution in the hillslope agroecosystem [7].

In dry conditions, subsurface hillslope flow is considered hydrologically horizontally disconnected, and the flow is primarily vertical, while under wet conditions, hillslopes are connected through subsurface lateral flow [8–10]. During periods of low evapotranspiration and low rainfall, high local convergence areas wet up and water moves downslope. Surface flow initiation occurs when the amount of water across the surface domain exceeds the infiltration capacity, causing excess water to flow over the soil surface as surface runoff. Surface vegetation cover, soil texture, soil porosity, soil structure (e.g., cracks, surface crusting), and compaction affect the infiltration of surface water [11]. Therefore, it is important to manage land use and soil conditions to maintain a high infiltration capacity and minimize runoff. Additionally, soil hydrophobicity, or the property of water repellence, can lead to reduced infiltration of water into the ground, which can increase the flow of surface water [12]. A rapid increase in potential evapotranspiration (and a decrease in rainfall) in the wet-to-dry condition transition, causes the soil to dry out and lateral flow will be reduced or even be stopped [8]. Downward flow into the soil profile as well as lateral subsurface flow greatly control the soil water content at a given location along the hillslope, and consequently the water availability for plants within the effective root zone. The ability to extract soil water is intrinsic for plants and the extent of water extraction depends on the plant type [13]. Furthermore, the actual water content of the soil influences nutrient availability for plants, but also aeration, which in turn may also affect biogeochemical processes [14].

Unsaturated soil hydraulic properties (SHPs) are essential for describing and predicting water flow in the unsaturated zone [15], but their parametrization is often not the aim itself, rather that they are essential for simulating water flow and transport processes [16]. One way of obtaining these properties is by laboratory measurements, which are commonly employed due to their reliability and acceptance [17–19]. However, laboratory-obtained SHPs may not always accurately represent field conditions and it is important to consider the limitations of laboratory-obtained SHPs in field modeling [20]. Factors such as soil structure can vary significantly under field conditions, leading to variations in SHPs. For example, soil structure may be altered by tillage or compaction [21]. Additionally, SHPs may be influenced by processes that are difficult to replicate in the laboratory, such as hysteresis. Hysteresis refers to the non-linear relationship between soil moisture content and water potential, which can lead to differences in the soil's ability to absorb and release water depending on its previous soil water content, and this effect cannot captured by the desiccation method commonly used in the laboratory measurements [22,23]. SHPs are generally measured at the smaller scale, which may not accurately represent the properties at the representative elementary volume (REV) which can lead to discrepancies in hydrological modeling at the field scale [20].

Furthermore, detailed soil campaigns are not always available or even feasible due to the complex nature/size of the area/system under investigation [24]. Measurements of the SHPs are often time-consuming and costly, and are subject to measurement errors [24], which creates a need for alternative parameter estimation procedures. In order to overcome the problematic lab measurements, pedotransfer functions (PTFs) have been developed, which are able to estimate the SHPs from easily obtainable soil parameters [15,25]. Unfortunately, when PTFs are applied outside the area they were calibrated for, they might result in predictions with limited accuracy [15], and therefore it is recommended to analyze which PTF is suitable for the site under investigation to reduce prediction errors. Another way to reduce the generalization error of the prediction might be ensemble modeling. Ensemble modeling is hereby the approach of predicting an outcome by using multiple inputs from the individual PTFs. In general, ensemble modeling is widely used in practical data science applications [26–29].

This study was conducted by combining field monitoring of soil and crop dynamics, laboratory measurements of soil hydraulic properties and characteristics, and numerical simulations with aim to answer the following research question of how good different methods for determining soil hydraulic properties (individual PTF, PTF model ensemble mean, laboratory evaporation method, and by field data from the sensor network) represent water flow dynamics along the different hillslope positions. Furthermore, it was tested if the usage of PTF ensemble mean could provide better results than individual PTFs at the investigated site.

2. Materials and Methods

2.1. Site Description

The investigations were conducted at the SUPREHILL Critical Zone Observatory (CZO) located in a hillslope vineyard at the experimental field Jazbina (45°51′24″ N, 16°00′22″ E) in Zagreb, Croatia. The hillslope is southwest exposed, and the vineyard rows are oriented along the slope. The hillslope is separated into three segments: hilltop, backslope, and footslope. In this 15-year-old vineyard, the soil type is classified as Dystric (Luvic) Stagnosol (IUSS Working Group WRB, Washington, DC, USA, 2014) [30] (Table 1).

Table 1. Average soil texture and organic carbon content (C_{org}) at the hilltop, backslope, and footslope for three depths (0–30, 30–60, and 60–90 cm) with standard deviation (SD), and soil type at the SUPREHILL CZO.

Position	Depth (cm)	Sand (%)	SD	Silt (%)	SD	Clay (%)	SD	C_{org} (g kg^{-1})	SD	USDA	Soil Type (IUSS, 2014)
Hilltop	0–30	5.7	1.5	71.0	1.0	23.3	0.6	11.9	0.5	silt loam	Dystric Luvic Stagnosol (Aric, Humic, Endoloamic, Episiltic)
	30–60	4.7	1.2	69.0	2.0	26.3	1.2	5.9	0.6	silt loam	
	60–90	7.3	0.6	60.3	7.4	32.3	6.8	2.0	0.6	silt clay loam	
Backslope	0–30	6.7	0.6	70.0	1.0	23.3	0.6	9.8	1.3	silt loam	Dystric Stagnosol (Aric, Colluvic, Humic, Inclinic, Siltic)
	30–60	8.3	3.2	67.3	3.1	24.3	1.5	6.1	0.4	silt loam	
	60–90	16.7	2.1	56.0	6.2	27.3	5.5	2.5	0.9	silt clay loam	
Footslope	0–30	6.7	1.5	75.0	3.0	18.3	4.5	12.4	1.2	silt loam	Dystric Stagnosol (Aric, Husmic, Inclinic, Siltic
	30–60	7.0	0.0	72.0	6.0	21.0	6.0	8.1	1.7	silt loam	
	60–90	6.3	0.6	67.7	5.5	26.0	5.6	4.7	1.1	silt loam	

2.2. Field Measurements, Weather and Crop Data

For the measurement of soil water content (SWC) TEROS 10/TEROS 12 (METER Group, Inc., Pullman, WA, USA) capacitance sensors were used. Sensors were installed at the different slope positions (hilltop, backslope, and footslope) with three replicates on three consecutive vine rows (with buffer rows in between) at two different soil depths (40 and 80 cm). Sensors were installed in between two vines (within an equal distance), in the observed vine rows, with three replicates in three vine rows, at two different soil depths (40 and 80 cm) at the different slope positions (hilltop, backslope, and footslope). In between each observed row, one non-observed vine row served as a buffer zone. For the observation of soil water potential (SWP) TEROS 21 sensors (METER Group, Inc., Pullman, WA, USA) were used in three repetitions in the nearby proximity of the SWC sensors, also at 40 and 80 cm depth (Figure 1). Both SWC and SWP sensor data were recorded at an hourly interval.

Weather data (air temperature, relative humidity, vapor and air pressure, solar radiation, wind speed and direction) was acquired from a meteorological station (ATMOS41, METER Group, Inc., Pullman, WA, USA) installed at the backslope. For the precipitation data, a mean value of measured rainfall and non-rainfall water (i.e., dew) using two high-precision weighable lysimeters (SFL 900, METER Group, Inc., Pullman, WA, USA) installed at hilltop and footslope was used. The raw lysimeter data underwent an extensive manual and automated plausibility control, as described in [31,32], before the subsequent

smoothing of the lysimeter data to reduce the impact of noise. To smooth the data and improve data reliability, the AWAT-filter was used, that applies an adaptive smoothing window size and adaptive threshold value [33–35].
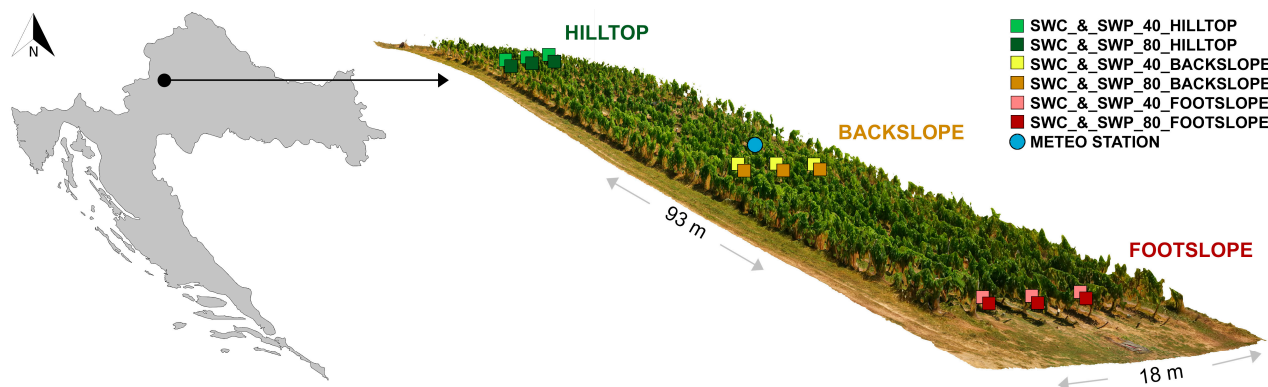

Figure 1. Location of the established SUPREHILL critical zone observatory (CZO) on the map of Croatia and the installed equipment setup at the hilltop, backslope and footslope presented on a 3D generated vineyard model (model generated in Agisoft Metashape based on UAV imagery).

The maximum assumed (moment of summer vine pruning (Figure 2)) canopy leaf area index (LAI) was measured by defoliation of the linear row distance (1 m of the row length) from the three representative vines of the vineyard. The selected vines (row length) were defoliated, all leaves were collected, and leaf samples were imaged using CropReporter (PhenoVation B.V., Wageningen, The Netherlands). Detailed description of the CropReporter™ is given in [36]. The leaf area for individual leaves, as well as for all sampled leaves, was calculated by DA software (PhenoVation B.V., Wageningen, The Netherlands), and a mean out of three samples was calculated.
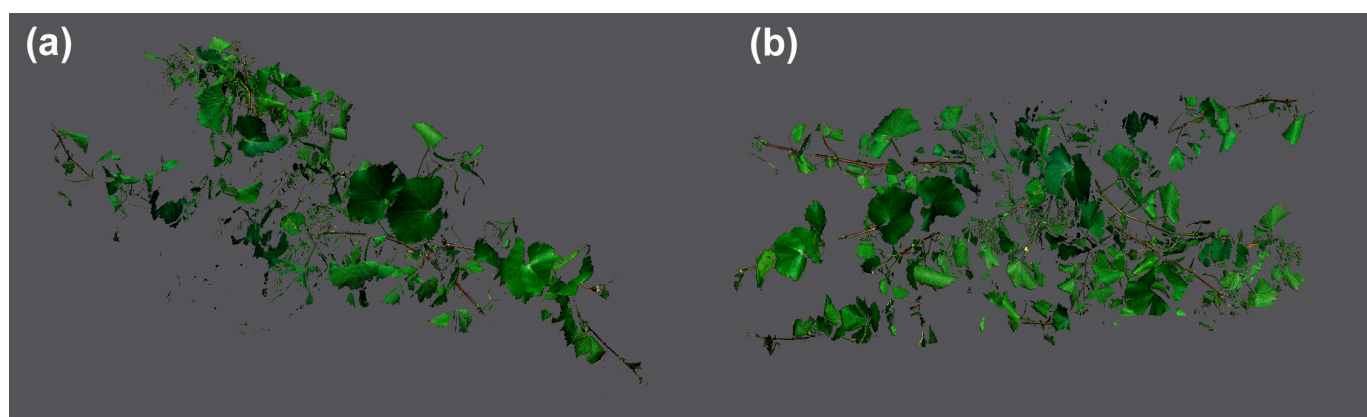
Figure 2. Exemplary display (3D model) of the representative vine (obtained with PlantEye F500 multispectral 3D scanner (Phenospex, Heerlen, The Netherlands)) at the SUPREHILL CZO at assumed maximum Leaf Area Index (LAI); (**a**) side view; (**b**) top view.

2.3. Soil Investigation and Soil Hydraulic Properties Datasets

Disturbed soil samples were taken from three positions (hilltop, backslope, and footslope) from three soil depths (0–30, 30–60, 60–90 cm), and three vine rows to determine the soil texture and organic carbon content (C_{org}). Soil texture was determined by combined wet sieving and sedimentation (ISO 11277:2009) (sand: 2–0.063 mm; silt: 0.063–0.02 mm; and clay: <0.002 mm), and the C_{org} by sulfochromic oxidation (ISO 14235:1998) (Table 1).

Based on field soil data, a number of widely used pedotransfer functions (PTFs), namely Carsel & Parrish [37], two versions of Rosetta [38], Woesten [39], Rawls [40], Weynants [41], and two versions of Toth [42] were used to estimate the properties of the soil

water retention curve and the saturated hydraulic conductivity for the model input data. The reason why a set of commonly applied PTFs has been used can be found in [24], where the authors showed, that the model outcome depends on the PTF selected. Therefore, a PTF based model mean might reproduce best results. Based on the HYDRUS results, a model ensemble consisting of the mentioned eight PTFs was produced to represent the PTF dataset. This procedure was repeated for each individual row, position, and depth available along the hillslope, while only the average soil data, representing the hillslope position are presented in Table 1.

A second set of simulations was performed based on the laboratory derived SHPs where undisturbed soil cores (250 cm^3) have been sampled at the hilltop, backslope, and footslope in three vineyard rows and in triplicates per location, at depths 0–20, 20–40, 40–60, and 60–90 cm, corresponding to the sensor-based monitoring network. Saturated hydraulic conductivity (K$_s$) was measured by the falling head method using the KSAT device (METER Group, Inc., Pullman, WA, USA). Furthermore, the same undisturbed soil cores were used for estimating SHPs by using the simplified evaporation method using the HYPROP system [43] in combination with the dewpoint device WP4C (both METER Group, Inc., Pullman, WA, USA) [44]. The fitted soil water retention curves (SWRCs) of the samples, as well as SHPs, were determined using the HYPROP-FIT software (METER Group, Inc., Pullman, WA, USA).

A third set of simulations dataset was generated by optimizing the parameters of the van Genuchten Mualem model (θ_r, θ_s, α and n) to the measured field soil water retention data using the Shuffled complex Evolution (SCE) algorithm (R package SoilHyP [45]). Field soil-water retention data were taken from parallel observations of SWC and SWP measurements in 40 and 80 cm soil depth. The SCE approach has been already used to estimate the SHPs from field experiments as it is suitable to find the correct parameters in the complex parameters space [45–47]. No measurements of the field soil-water retention curve were available for the first and third depth (0–20 and 40–60 cm). Thus, parameters for θ_r, θ_s, α, n and K$_s$ were taken from laboratory measurements to parameterize the first and third layer of the soil profile.

2.4. Numerical Modeling

Water flow was simulated using the HYDRUS-1D software [48] (version 4.17.0140). For the simulation of water flow the Richards equation for the variably saturated porous medium was solved and can be written as:

$$\frac{\partial \theta}{\partial t} = \frac{\partial}{\partial z} K \left(\frac{\partial h}{\partial z} + 1 \right) - S \tag{1}$$

where θ is volumetric soil water content [L^3 L^{-3}], h is pressure head [L], K is hydraulic conductivity of unsaturated soil [L T^{-1}], z is the gravitational head [L], t is time [T], and S is a sink term for root water uptake [T^{-1}].

Soil hydraulic functions were described using the van Genuchten-Mualem single porosity model [49]:

$$\theta(h) = \begin{cases} \theta_r + \dfrac{\theta_s - \theta_r}{(1 + |\alpha h|^n)^m} & h < 0 \\ \theta_s & h \geq 0 \end{cases} \tag{2}$$

$$K(h) = K_s S_e^l \left(1 - \left(1 - S_e^{\frac{1}{m}} \right)^m \right)^2 \tag{3}$$

$$S_e = \frac{\theta - \theta_r}{\theta_s - \theta_r} \tag{4}$$

$$m = 1 - \frac{1}{n}; \ n > 1 \tag{5}$$

where $\theta(h)$ is volumetric water content [L^3 L^{-3}], $K(h)$ is hydraulic conductivity of unsaturated soil at the water pressure head of h [L], θ_r is residual soil-water content [L^3 L^{-3}], θ_s is

water content at saturation [$L^3 L^{-3}$], S_e is the effective saturation [-], K_s is the saturated hydraulic conductivity of the soil [$L T^{-1}$], α is the inverse of air-entry value (bubbling pressure) [L^{-1}], n is the dimensionless soil pore size distribution index [-], m is the dimensionless optimization coefficient [-], and l is the pore connectivity parameter [-].

Boundary conditions for the simulations were set to atmospheric conditions (daily data) with surface runoff at the top, while a free drainage was applied for the bottom. Domain discretization density was increased near the soil surface with a total number of 150 nodes for the 150 cm deep simulation domain. The soil profile was initialized in water content according to the measured water contents at the different locations at the beginning of the simulation time.

Evapotranspiration of vine (ET_c) was calculated using the reference evapotranspiration (ET_0) determined with the Penman–Monteith equation [50] and FAO crop coefficients ($K_{c\ ini}$: 0.3; $K_{c\ mid}$: 0.7 and $K_{c\ end}$: 0.45) [51]. The assumed LAI development stages correspond with used K_c stages. A simplified LAI approach was used, assuming a linear increase in the early developing stages until measured maximum at summer pruning (LAI_{max}: 3.55), following a 20% decrease (due to vine biomass cut) with constant values until the end of mid stage (7 June 2021), and a linear decrease until the end of the late stage (30 September 2021).

Root water uptake was simulated using the approach of Feddes et al. (1978) setting the parameters *P0* to −10 cm, *POpt* to −25 cm, *P2H* to −400 cm, *P2L* to −500 cm, and *P3* to −8000 cm, corresponding for the parameter set available for grapes in the HYDRUS integrated library. Maximum rooting depth was set at 100 cm based on field observations.

2.5. Statistical Analysis

Model performance was evaluated using the mean absolute error (*MAE*), root mean square error (*RMSE*), mean absolute percentage error (*MAPE*), and coefficient of determination (R^2):

$$MAE = \frac{\sum_{i=1}^{N}|P_i - O_i|^2}{N} \tag{6}$$

$$RMSE = \sqrt{\frac{\sum_{i=1}^{N}(P_i - O_i)^2}{N}} \tag{7}$$

$$MAPE = \frac{1}{N}\sum_{i=1}^{N}\left|\frac{O_i - P_i}{O_i}\right| \tag{8}$$

$$R^2 = \frac{\sum_{i=1}^{N}\left(O_i - \overline{O}\right)\left(P_i - \overline{P}\right)}{\left[\sum_{i=1}^{N}\left(O_i - \overline{O}\right)^2\right]^{0.5}\left[\sum_{i=1}^{N}\left(P_i - \overline{P}\right)^2\right]^{0.5}} \tag{9}$$

where O_i is observation, P_i is prediction, $\bar{O}$ is average observation and $\overline{P}$ is average prediction, while N is the sample size.

Seasonal SWC was evaluated using the coefficient of variation (*CV*):

$$CV = \frac{SD}{\overline{O}} \times 100 \tag{10}$$

where *SD* is standard deviation and $\bar{O}$ is average observation.

3. Results

3.1. Laboratory and Field Soil Water Retention Characteristics

The laboratory obtained parameters showed that the saturated water content (θ_s) (Table 2) varied from 0.32 cm^3 cm^{-3} (backslope (row III) at 60–90 cm) to 0.44 cm^3 cm^{-3} (footslope (row II) at 40–60 cm). The K_s values varied from 0.08 cm day^{-1} (backslope row I at 0–20 cm) to high as 82.6 cm day^{-1} (hilltop row II) at 60–90 cm). At the hilltop and backslope, θ_s (Table 2), was generally decreasing with depth, while bulk density was increasing, agreeing with previous findings at similar sites [52,53]. Average C$_{org}$ (Table 1)

ranged from 12.4 g kg^{-1} (footslope at 0–30 cm) to 2 g kg^{-1} (hilltop at 60–90 cm) and was decreasing with depth at each hillslope position. Bulk densities varied from varied from (1.75 g cm^{-3}) (backslope (row III) at 60–90 cm) to 1.42 g cm^{-3} (hilltop (row III) at 0–20 cm). Furthermore, the lowest θ_s (0.32 cm^3 cm^{-3}) corresponded with the highest bulk density of a sample at the site. Values of RMSE (θ) < 0.03 cm^3 cm^{-3} (Table 2) indicated the applicability of VGM for all locations. In the undisturbed soil samples sampled at the hilltop and backslope positions (depth of 60–90 cm), soil concretions and gravel was found that could cause higher K_s and lower θ_s values due to the lack of possibility for water retention. The footslope position generally had the lowest K_s, and range of values. Figure 3 shows exemplary differences in SWRCs at different hillslope positions, depths, rows, and soil cores.

Table 2. van Genuchten-Mualem (VGM) hydraulic properties evaluated by HYPROP-FIT for the hilltop, backslope, and footslope for four depths (0–20, 20–40, 40–60, and 60–90 cm) and three vineyard rows at the SUPREHILL CZO.

| Position	Row	Depth (cm)	θ_r (cm^3 cm^{-3})	θ_s (cm^3 cm^{-3})	α (cm^{-1})	n (-)	K_s (cm day^{-1})	RMSE (θ)	Bulk Density (g cm^{-3})
Hilltop	I	0–20	0	0.39	0.00445	1.201	0.38	0.018	1.52
		20–40	0	0.38	0.00537	1.182	1.04	0.013	1.54
		40–60	0	0.38	0.0071	1.171	1.83	0.016	1.59
		60–90	0.103	0.37	0.00618	1.229	1.01	0.009	1.63
	II	0–20	0	0.42	0.00667	1.185	0.79	0.011	1.48
		20–40	0	0.40	0.0052	1.178	1.37	0.013	1.51
		40–60	0	0.35	0.013	1.109	18.70	0.011	1.71
		60–90	0	0.40	0.0319	1.112	82.60	0.015	1.56
	III	0–20	0	0.42	0.00329	1.238	0.26	0.010	1.42
		20–40	0	0.39	0.0104	1.151	2.71	0.016	1.5
		40–60	0	0.35	0.00995	1.112	6.76	0.014	1.71
		60–90	0.21	0.37	0.00718	1.389	0.31	0.015	1.65
Backslope	I	0–20	0	0.37	0.00428	1.190	0.42	0.012	1.61
		20–40	0	0.39	0.00877	1.143	9.31	0.022	1.56
		40–60	0.172	0.34	0.00702	1.317	0.39	0.012	1.7
		60–90	0.214	0.34	0.00524	1.508	0.08	0.013	1.74
	II	0–20	0	0.38	0.00395	1.222	0.22	0.011	1.59
		20–40	0	0.37	0.00576	1.181	1.20	0.015	1.55
		40–60	0	0.39	0.00627	1.177	2.34	0.014	1.58
		60–90	0	0.35	0.0186	1.124	18.50	0.011	1.69
	III	0–20	0	0.37	0.00603	1.162	0.95	0.029	1.6
		20–40	0	0.37	0.00252	1.278	0.41	0.010	1.51
		40–60	0.144	0.34	0.00806	1.320	1.16	0.014	1.68
		60–90	0.167	0.32	0.00569	1.445	0.28	0.011	1.75
Footslope	I	0–20	0	0.39	0.00737	1.194	1.59	0.009	1.46
		20–40	0	0.39	0.00599	1.210	1.25	0.008	1.5
		40–60	0	0.41	0.00317	1.257	0.79	0.018	1.53
		60–90	0	0.42	0.00447	1.179	2.09	0.018	1.51
	II	0–20	0	0.37	0.0036	1.233	0.25	0.010	1.54
		20–40	0	0.37	0.00469	1.218	0.46	0.011	1.54
		40–60	0	0.44	0.00344	1.249	0.94	0.016	1.45
		60–90	0	0.43	0.00251	1.229	0.77	0.009	1.47
	III	0–20	0	0.39	0.00357	1.211	0.53	0.009	1.53
		20–40	0	0.38	0.00331	1.235	0.52	0.013	1.58
		40–60	0.016	0.42	0.00967	1.158	8.24	0.012	1.49
		60–90	0	0.43	0.00458	1.180	1.51	0.016	1.48
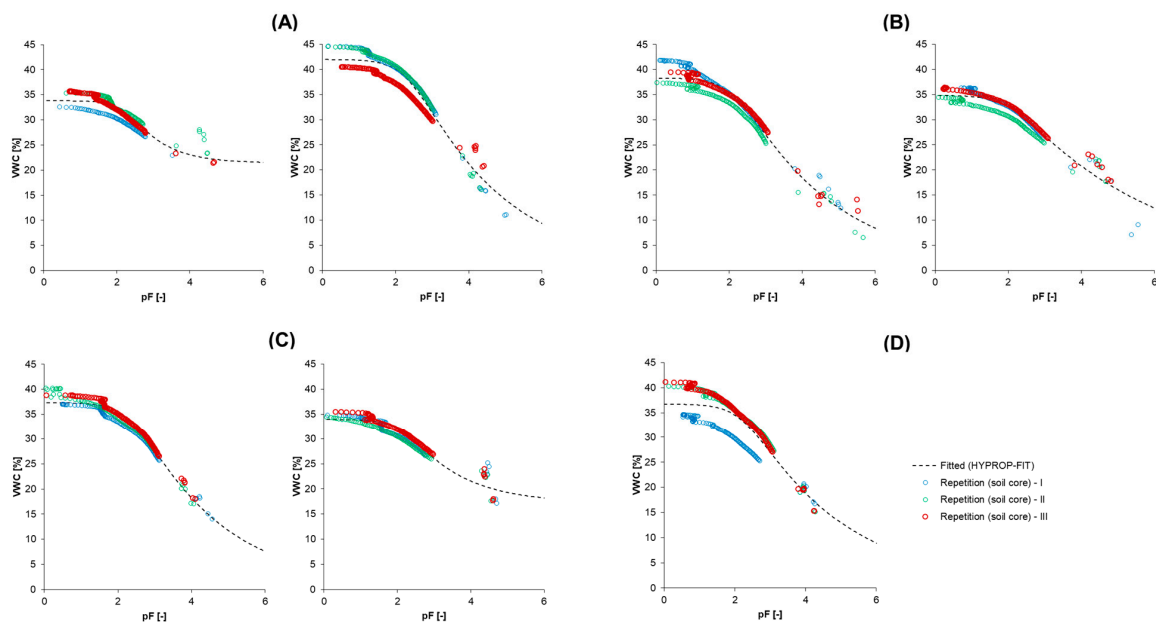
Figure 3. Exemplary differences in soil water retention points and curves obtained in the laboratory by the evaporation method and fitted soil water retention curve with three repetitions each (Repetition (I) to Repetition (III)) for: (**A**) different positions at the same row and depth: backslope and footslope (row I) at 60–90 cm; (**B**) different rows at the same depth and position: hilltop (row I & row II) at 40–60 cm; (**C**) different depth at the same row and position: backslope at 0–20 cm and 40–60 cm (row I); and (**D**) one location, depth and position: backslope at 0–20 cm (row III) at the SUPREHILL observatory.

Even if smaller differences were found between the triplicates from each sample location (depth and row) larger differences between the retention characteristics were found between the sampled rows (Figure 3). The stated soil heterogeneity is confirmed with field data, where the differences are more noticeable (Figure 4) for rows and hillslope positions.
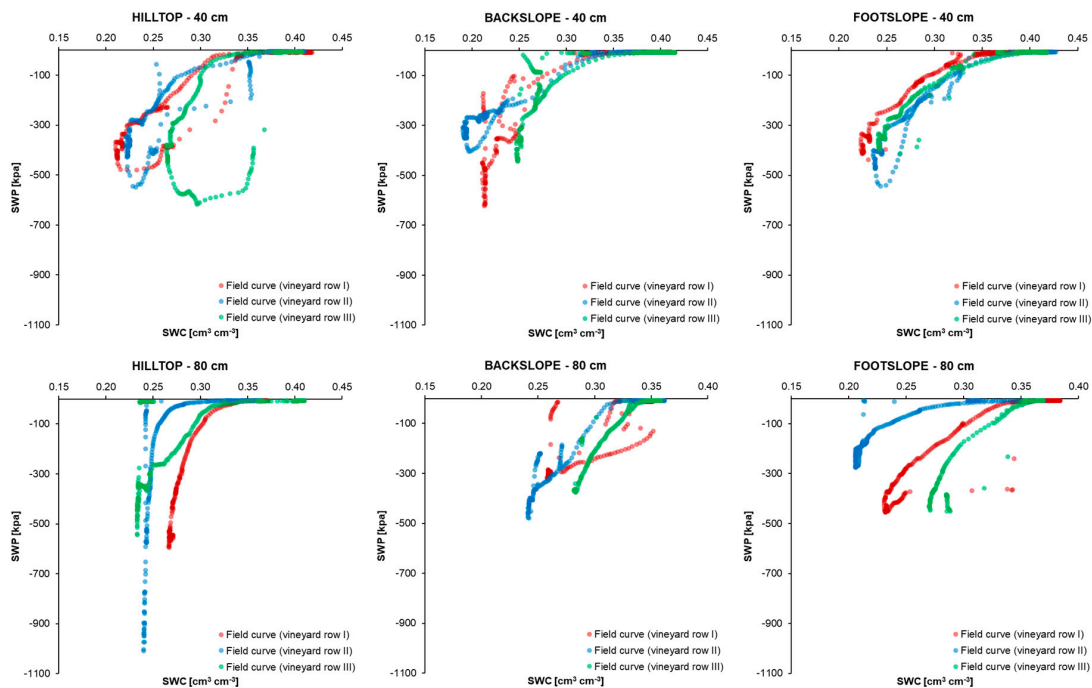

Figure 4. Measured soil water content (SWC) [cm^3 cm^{-3}] and soil water potential (SWP) (daily data) at two depths (40 and 80 cm) in three repetitions (vineyard rows) in 2021 at the SUPREHILL CZO.

3.2. Model Results

As mentioned, three different inputs in soil hydraulic properties were estimated, either based on pedotransfer functions, laboratory measurements, or parameter estimation based on sensor network data and then the SHPs estimated/determined were propagated through the hydrological simulator HYDRUS-1D (Figures 5 and 6).

Figure 5. Simulated soil water content (SWC) [cm^3 cm^{-3}] in HYDRUS-1D: pedotransfer (PTF) model ensemble (red line), PTF model ensemble spread (5–95 percentile range) (grey area), laboratory dataset (dashed black line) and combination of lab and field data (black line), and field SWC measurements (blue line) in three vineyard rows at 40 cm depth, with precipitation data obtained with weighing lysimeter in 2021 at the SUPREHILL Critical Zone Observatory.
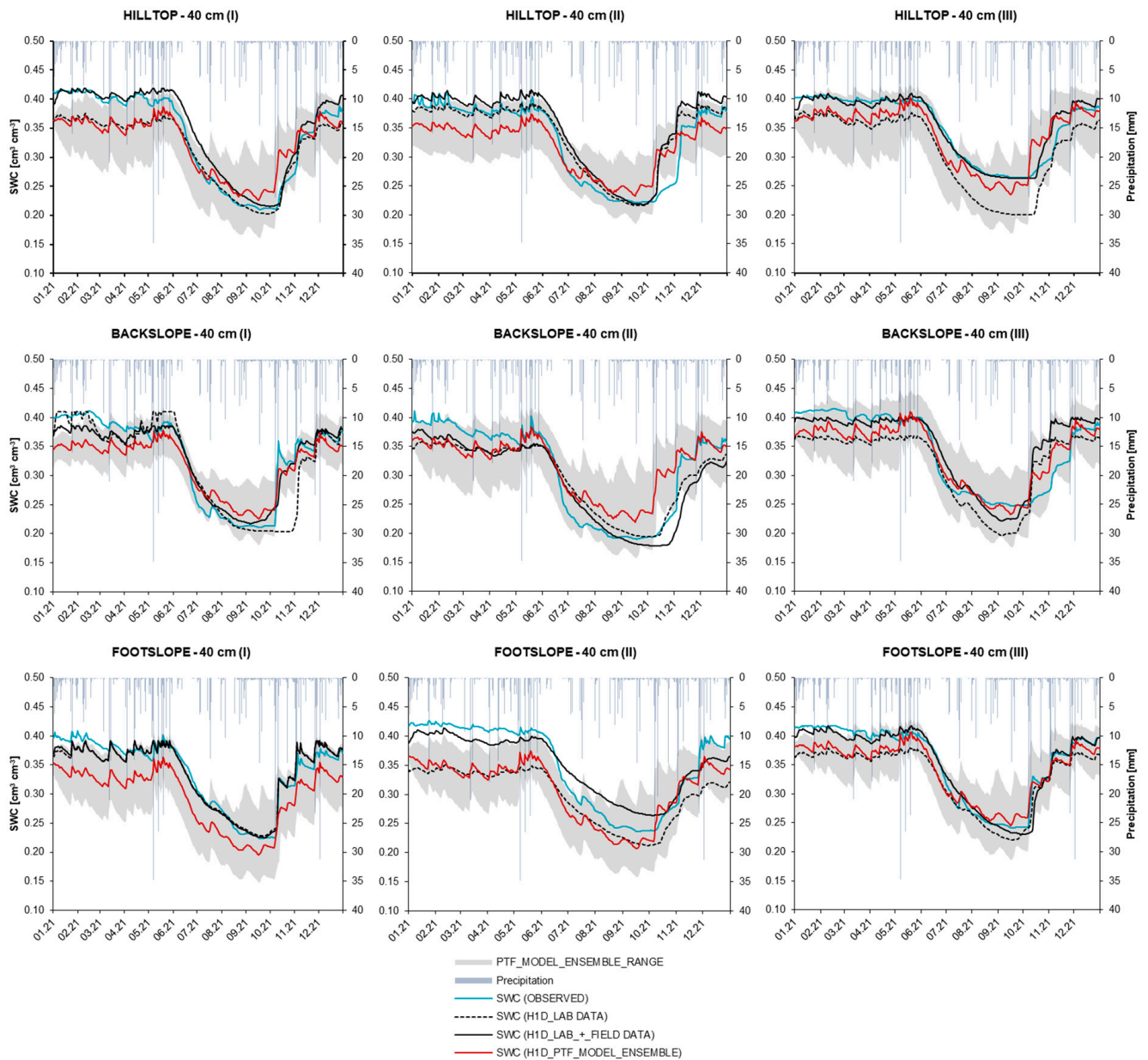
Figure 6. Simulated soil water content (SWC) [cm^3 cm^{-3}] in HYDRUS-1D: pedotransfer (PTF) model ensemble (red line), PTF model ensemble spread (5–95 percentile range) (grey area), laboratory dataset (dashed black line) and combination of lab and field data (black line), and field SWC measurements (blue line) in three vineyard rows at 40 cm depth, with precipitation data obtained with weighing lysimeter in 2021 at the SUPREHILL Critical Zone Observatory.
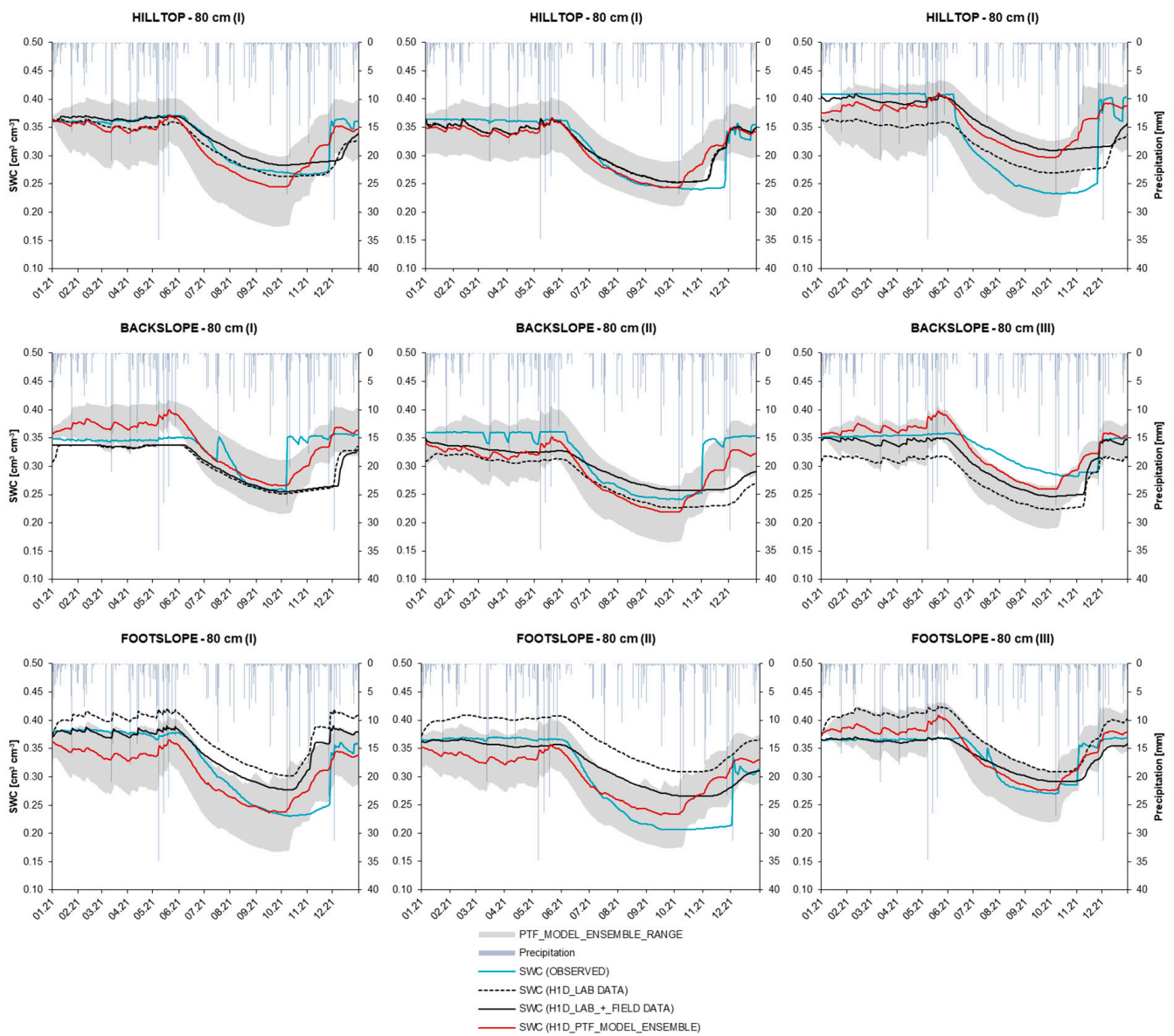
The highest agreement of simulated values with measured SWC for 40 cm soil depth was found with the laboratory + field data, with the lowest average MAE, RMSE and MAPE (0.02, 0.02 and 5.34%, respectively), and highest average R^2 (0.93) (Table 3). At 40 cm soil depth, the highest average MAE, RMSE and MAPE (0.07, 0.08 and 27.52%) was found for an individual PTF—Carsel & Parrish dataset, while the lowest average R^2 (0.81) was found for an individual PTF—Toth, continuous dataset. For the 40 cm soil depth, PTF model ensemble did not perform better (MAE = 0.03, RMSE = 0.03, MAPE = 9.41%, R^2 = 0.9) over the best performed individual PTF—Weynants (MAE = 0.02, RMSE = 0.03, MAPE = 7.64%, R^2 = 0.92).

Table 3. Mean absolute error (MAE), root mean square error (RMSE), mean absolute percentage error (MAPE) and coefficient of determination (R^2) for simulated SWC (individual PTFs, PTF model ensemble, laboratory data, and laboratory + field data) vs. observed SWC at 40 and 80 cm soil depth in 2021 at the SUPREHILL CZO.

		40 cm										80 cm									
		HILLTOP			BACKSLOPE			FOOTSLOPE				HILLTOP			BACKSLOPE			FOOTSLOPE			
		ROW										ROW									
		I	II	III	I	II	III	I	II	III	Mean	I	II	III	I	II	III	I	II	III	Mean
PTF Carsel & Parrish	MAE	0.09	0.04	0.11	0.04	0.06	0.05	0.09	0.10	0.06	**0.07**	0.08	0.02	0.09	0.03	0.07	0.03	0.08	0.06	0.03	**0.05**
	RMSE	0.10	0.04	0.11	0.04	0.07	0.05	0.09	0.11	0.06	**0.08**	0.09	0.02	0.10	0.03	0.07	0.03	0.08	0.07	0.03	**0.06**
	MAPE	35.84	12.15	45.05	12.02	25.10	16.72	37.80	42.84	20.19	**27.52**	36.16	5.99	37.56	8.90	31.05	9.52	33.07	24.47	9.29	**21.78**
	RSQ	0.85	0.89	0.80	0.91	0.86	0.84	0.91	0.81	0.93	**0.87**	0.73	0.77	0.77	0.65	0.88	0.67	0.71	0.68	0.84	**0.75**
PTF Rosseta	MAE	0.04	0.02	0.03	0.02	0.04	0.05	0.06	0.06	0.04	**0.04**	0.03	0.02	0.03	0.03	0.05	0.05	0.04	0.03	0.02	**0.03**
	RMSE	0.05	0.03	0.03	0.03	0.05	0.06	0.06	0.07	0.05	**0.05**	0.04	0.03	0.04	0.04	0.05	0.05	0.05	0.04	0.03	**0.04**
	MAPE	12.79	7.18	9.54	7.22	14.77	18.11	22.21	22.61	14.18	**14.29**	11.58	6.61	9.57	9.19	18.49	18.34	15.78	9.19	8.00	**11.86**
	RSQ	0.86	0.86	0.82	0.91	0.84	0.81	0.93	0.82	0.92	**0.86**	0.79	0.78	0.79	0.64	0.90	0.67	0.75	0.72	0.87	**0.77**
PTF Rosseta (+BD)	MAE	0.05	0.03	0.04	0.05	0.03	0.06	0.09	0.06	0.06	**0.05**	0.04	0.03	0.03	0.03	0.06	0.06	0.06	0.04	0.03	**0.04**
	RMSE	0.05	0.04	0.04	0.06	0.04	0.07	0.09	0.07	0.06	**0.06**	0.05	0.03	0.04	0.04	0.06	0.07	0.06	0.04	0.04	**0.05**
	MAPE	15.27	11.13	13.43	17.03	9.88	23.39	38.51	22.99	19.76	**19.04**	16.08	9.61	8.82	12.80	24.31	24.65	22.85	12.17	12.64	**15.99**
	RSQ	0.87	0.87	0.83	0.92	0.88	0.83	0.92	0.84	0.92	**0.88**	0.79	0.79	0.81	0.60	0.92	0.66	0.77	0.72	0.86	**0.77**
PTF Woesten	MAE	0.05	0.06	0.03	0.05	0.05	0.02	0.03	0.04	0.03	**0.04**	0.02	0.04	0.04	0.02	0.03	0.02	0.05	0.06	0.02	**0.03**
	RMSE	0.06	0.06	0.04	0.06	0.07	0.03	0.04	0.05	0.04	**0.05**	0.02	0.04	0.05	0.02	0.03	0.02	0.05	0.06	0.02	**0.04**
	MAPE	15.33	17.62	9.14	17.14	15.70	6.97	8.52	12.64	9.51	**12.51**	6.27	12.01	12.73	6.29	9.99	4.81	14.49	18.79	5.44	**10.09**
	RSQ	0.61	0.45	0.55	0.92	0.57	0.88	0.70	0.63	0.73	**0.67**	0.78	0.68	0.92	0.50	0.91	0.84	0.23	0.17	0.79	**0.65**
PTF Rawls	MAE	0.02	0.06	0.02	0.03	0.02	0.03	0.05	0.05	0.02	**0.03**	0.01	0.05	0.06	0.05	0.05	0.05	0.02	0.03	0.04	**0.04**
	RMSE	0.03	0.07	0.03	0.03	0.03	0.04	0.05	0.06	0.02	**0.04**	0.02	0.06	0.08	0.05	0.05	0.06	0.02	0.03	0.04	**0.05**
	MAPE	6.68	22.05	6.83	8.15	7.82	9.44	18.29	19.33	4.83	**11.49**	3.51	18.83	16.53	14.35	16.43	12.62	6.27	10.92	11.27	**12.30**
	RSQ	0.89	0.82	0.79	0.89	0.82	0.86	0.92	0.94	0.90	**0.87**	0.90	0.67	0.64	0.13	0.89	0.54	0.91	0.96	0.66	**0.70**
PTF Weynants	MAE	0.03	0.02	0.02	0.02	0.04	0.03	0.02	0.03	0.02	**0.02**	0.01	0.01	0.05	0.04	0.01	0.03	0.01	0.03	0.03	**0.03**
	RMSE	0.03	0.03	0.02	0.03	0.05	0.04	0.02	0.03	0.02	**0.03**	0.02	0.02	0.06	0.04	0.02	0.04	0.02	0.04	0.04	**0.03**
	MAPE	8.46	6.44	4.59	7.66	13.78	9.21	5.62	7.76	5.19	**7.64**	3.60	4.90	13.27	10.57	4.57	7.73	4.78	9.62	8.98	**7.56**
	RSQ	0.94	0.94	0.86	0.93	0.94	0.83	0.96	0.90	0.97	**0.92**	0.89	0.93	0.82	0.51	0.84	0.80	0.94	0.92	0.81	**0.83**
PTF Toth (class)	MAE	0.02	0.05	0.02	0.03	0.05	0.02	0.02	0.02	0.02	**0.03**	0.05	0.06	0.04	0.05	0.03	0.04	0.03	0.05	0.03	**0.04**
	RMSE	0.03	0.06	0.03	0.03	0.06	0.03	0.02	0.03	0.03	**0.03**	0.05	0.06	0.06	0.05	0.04	0.05	0.04	0.06	0.03	**0.05**
	MAPE	7.63	13.41	5.34	8.42	14.46	5.83	5.27	6.29	7.15	**8.20**	12.74	15.76	11.95	12.22	9.66	11.37	8.53	15.97	8.65	**11.87**
	RSQ	0.91	0.86	0.80	0.90	0.88	0.85	0.94	0.85	0.95	**0.88**	0.83	0.79	0.82	0.59	0.89	0.76	0.87	0.83	0.92	**0.81**

Table 3. *Cont.*

		40 cm										80 cm									
		HILLTOP			BACKSLOPE			FOOTSLOPE				HILLTOP			BACKSLOPE			FOOTSLOPE			
		ROW										ROW									
		I	II	III	I	II	III	I	II	III	Mean	I	II	III	I	II	III	I	II	III	Mean
PTF Toth (continuous)	MAE	0.04	0.03	0.02	0.04	0.06	0.05	0.02	0.04	0.03	**0.04**	0.02	0.02	0.05	0.03	0.01	0.03	0.03	0.04	0.04	**0.03**
	RMSE	0.05	0.04	0.04	0.05	0.08	0.06	0.03	0.04	0.04	**0.05**	0.03	0.03	0.06	0.03	0.01	0.04	0.04	0.05	0.05	**0.04**
	MAPE	12.23	10.19	6.36	11.67	17.44	12.86	7.57	11.41	8.74	**10.94**	5.53	6.13	12.95	7.85	2.56	9.47	8.32	11.80	10.84	**8.38**
	RSQ	0.82	0.81	0.68	0.92	0.83	0.76	0.88	0.74	0.86	**0.81**	0.68	0.65	0.63	0.69	0.93	0.64	0.60	0.56	0.84	**0.69**
PTF model ensemble	MAE	0.03	0.03	0.02	0.03	0.03	0.02	0.04	0.05	0.01	**0.03**	0.02	0.02	0.04	0.02	0.03	0.02	0.04	0.03	0.02	**0.03**
	RMSE	0.04	0.03	0.03	0.03	0.04	0.02	0.04	0.05	0.02	**0.03**	0.02	0.02	0.05	0.03	0.03	0.02	0.04	0.04	0.02	**0.03**
	MAPE	9.33	9.26	7.03	8.84	10.65	5.58	14.13	14.30	5.61	**9.41**	5.53	5.37	12.01	6.62	9.01	5.65	8.88	10.67	4.21	**7.55**
	RSQ	0.90	0.88	0.82	0.94	0.88	0.89	0.96	0.89	0.96	**0.90**	0.84	0.80	0.83	0.59	0.94	0.80	0.81	0.80	0.89	**0.81**
Laboratory data	MAE	0.02	0.01	0.04	0.02	0.03	0.04	0.01	0.05	0.03	**0.03**	0.01	0.01	0.04	0.03	0.04	0.05	0.05	0.07	0.04	**0.04**
	RMSE	0.03	0.02	0.04	0.04	0.03	0.04	0.01	0.06	0.03	**0.03**	0.02	0.02	0.05	0.04	0.05	0.05	0.06	0.07	0.04	**0.04**
	MAPE	6.30	5.10	12.39	6.91	8.24	10.76	3.20	13.92	7.04	**8.21**	3.26	4.76	12.75	8.12	12.83	14.94	18.04	26.50	11.17	**12.49**
	RSQ	0.97	0.90	0.97	0.78	0.93	0.76	0.95	0.97	0.97	**0.91**	0.86	0.91	0.83	0.35	0.56	0.83	0.77	0.95	0.83	**0.77**
Laboratory + field data (inverse)	MAE	0.02	0.02	0.01	0.01	0.03	0.02	0.01	0.02	0.01	**0.02**	0.01	0.01	0.04	0.03	0.03	0.02	0.03	0.03	0.01	**0.02**
	RMSE	0.02	0.03	0.01	0.02	0.03	0.03	0.01	0.02	0.02	**0.02**	0.02	0.02	0.05	0.04	0.04	0.03	0.04	0.04	0.02	**0.03**
	MAPE	5.10	8.01	2.25	4.64	8.56	7.34	2.97	6.58	2.63	**5.34**	4.21	4.76	15.12	7.82	9.40	6.99	9.95	12.72	3.73	**8.30**
	RSQ	0.97	0.91	0.95	0.95	0.91	0.77	0.95	0.96	0.96	**0.93**	0.78	0.92	0.73	0.62	0.53	0.86	0.79	0.94	0.81	**0.77**

At 80 cm soil depth, PTF model ensemble performed better (MAE = 0.03, RMSE = 0.03, MAPE = 7.55%, R^2 = 0.81) than other parameter sets used. Only higher R^2 (0.82) was found for the individual PTF—Weynants, and lower MAE (0.02) with the laboratory + field dataset. The lowest agreement of simulated values with measured SWC for 80 cm soil depth was found with the Carsel & Parrish, with the highest average MAE, RMSE and MAPE (0.05, 0.06 and 21.78%, respectively), and lowest average R^2 (0.75) (Table 3).

Lowest coefficient (0.3%) of variation (CV) for SWC at 80 cm soil depth was found at the footslope in winter and spring season in vineyard row III, while the lowest (1.8%) at 40 cm was found at the hillop in winter in row III (Figure 7). In general, lower CV for SWC was found at the 80 cm soil depth. At the soil depth of 40 cm, the highest (25%) CV was found in autumn at the backslope in row II, while at 80 cm, the highest (24.6) was found at the hilltop in row III, also in autumn. Overall, highest CVs were found in autumn, during the soil rewetting phase.
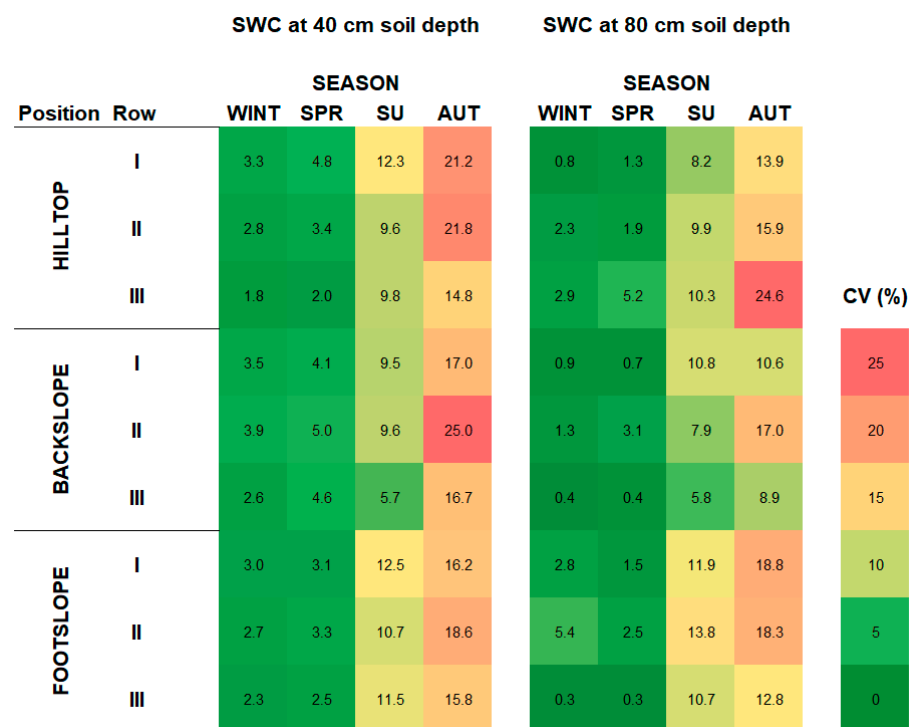
Figure 7. Heatmap of coefficients of variation (CV) [%] for soil water content (SWC) at the at two depths (40 and 80 cm), in three vineyard rows, along the hillslope (hilltop, backslope and footslope) in 2021 at the SUPREHILL Critical Zone Observatory.

4. Discussion

Variations in soil properties can significantly impact the hydrological processes by affecting water infiltration, storage, and flow. This can cause differences in the amount of water retained in the soil, leading to variable runoff generation at the hillslope [54,55]. Soil heterogeneity can result in differential water uptake, leading to variable soil water content and rates of rewetting. It is widely known that vertical and lateral soil heterogeneities are not uncommon in intensively used agroecosystems, as land use and soil management practices impact the soils directly. At the hillslope scale additional processes such as soil erosion and deposition contribute to the soil development and lead to heterogeneities [56]. These can lead to strong changes in water and solute transport, as well as biomass development, along the hillslope scale [57]. At the pedon scale itself, structural heterogeneity may lead to preferential flow through macropores, cracks, and intra-aggregate pore spaces causing flow instabilities [58], resulting in a reduction in the residence time of the percolating soil water [56] and nonuniform water flow through the profile. Therefore, the shape of the retention characteristics, especially in the wet and mid water saturated range (100–1000 cm)

is of particular importance for the investigation of hydrological response of soils [59]. On the other hand, other processes such as hydrophobicity and wettability of the soil (surface), are classically not represented in the retention characteristics (drying branch) but may also cause preferential flow [60].

Looking at the field retention data by plotting field measured SWCs versus measured SWP at the same location and depth (Figure 4), a more detailed picture can be drawn. First, at some locations a clear hysteresis between wetting and drying cycle can be detected, which is most prominent for the hilltop position and measurements at 40 cm depth. The assumption made is here that the measured water potential is in equilibrium with the progressing water front. Additionally, the data are much noisier due to different response times of the sensors and/or small scale soil heterogeneities as already detectable in the data from the laboratory.

Hillslope hydrological processes are influenced by variations in hillslope SWC, while the complexity and heterogeneity of water movement, makes it often difficult to predict temporal and spatial processes and patterns [61], and the presented data exhibits the mentioned. Field sensor measurements captured SWC variability during rewetting phase, for different vineyard rows, hillslope positions and depths. These differences were most pronounced in the deeper layer, suggesting that in the rewetting process the impact of lateral flow is dominant in some cases (Figure 6).

Islam et al. [62] compared actual SWC to three sets of simulated values that were generated using three different sets of hydraulic parameters, and found that the model is accurate only if the soil hydraulic parameters are estimated using site-specific PTFs, but noted that none of the methods used can accurately simulate soil water content data, so the most accurate method is still unknown. Gijsman et al. [63] compared eight methods of estimating hydraulic parameters using a functional approach for predicting crop yield and found that the differences between estimations were significant, making it difficult to determine which method is best for specific soils. Baroni et al. (2010) [64] in a similar study, demonstrated that soil hydraulic properties obtained by direct methods do not necessarily guarantee the best results. The use of PTFs based on site-specific texture and organic matter data did indeed provide comparable simulation results for the given experimental profile. Even though similar approaches and combinations of methods are used in research, data is often not validated on a rather dynamic hydrological system such as a hillslope.

PTF model ensemble in some cases captured the observed soil water dynamics well (e.g., backslope [row I, 40 cm] or footslope [row I, 40 cm]) (Figure 5), but could not reproduce water contents near saturation as also shown for the soil hydraulic characterization based on laboratory data. Additionally, a downside of the laboratory dataset could be observed in the drying out phase (e.g., hilltop [row III, 40 cm], backslope [row III, 40 cm], or footslope [row II, 40 cm]), as the SWC response in simulations did not agree with field SWC measurements in a timely manner. Nevertheless, the dataset using field data was the only one that could capture soil water dynamics near saturation in general (Figure 6). Our model performance results point out that in absence of field or laboratory data, for this field conditions and site, the generated PTF model ensemble could as well as be used as a reliable method at the investigated site.

5. Conclusions

In the absence of laboratory-estimated soil hydraulic properties (SHPs), the presented data indicated that model ensemble using PTFs (or even certain individual PTFs) could be considered reliable, for this site and conditions. Even though laboratory-estimated SHPs provided relatively dependable values, better model performance was achieved with the same dataset after the sensor network estimated SHPs were incorporated into the dataset. Furthermore, model performance evaluation with different statistical parameters was needed for adequate assessment. Field observations indicated that heterogeneity and spatial variability regarding soil parameters were present at the site. Soil water content acted in a heterogeneous manner in both space and time across the hillslope. Due to the

nature of the water flow of the sloped site, two- or three-dimensional modeling could provide more sufficient data due to spatial variables and complex hydrological processes involved in future research at the site. For future investigation, modeling could provide better results, but considering this kind the vineyard is a multi-crop system (grass & vine), the whole system should be accounted for, as well as more detailed crop observations.

Author Contributions: Conceptualization, V.K., J.G., L.W. and V.F.; Data curation, V.K.; Formal analysis, V.K., J.G., L.W. and J.D.; Funding acquisition, L.F. and V.F.; Investigation, V.K., L.F., J.D., Z.K., I.M. and V.F.; Methodology, V.K., J.G., L.W. and V.F.; Project administration, V.K., L.F. and V.F.; Resources, L.F.; Software, V.K., J.G., L.W., J.D. and B.L.; Supervision, V.F.; Visualization, V.K.; Writing—original draft, V.K.; Writing—review & editing, J.G., L.W., L.F., Z.K., I.M., B.L., T.B. and V.F. All authors have read and agreed to the published version of the manuscript.

Data Availability Statement: Data available on demand.

Conflicts of Interest: The authors declare no conflict of interest.

References

1. Dusek, J.; Vogel, T. Modeling travel time distributions of preferential subsurface runoff, deep percolation and transpiration at a montane forest hillslope site. *Water* **2019**, *11*, 2396. [CrossRef]
2. Nanda, A.; Sen, S.; Sharma, A.N.; Sudheer, K.P. Soil temperature dynamics at hillslope scale-field observation and machine learning-based approach. *Water* **2020**, *12*, 713. [CrossRef]
3. Lopes, I.; Montenegro, A.A.A.; de Lima, J.L.M.P. Performance of conservation techniques for semiarid environments: Field observations with caatinga, Mulch, and Cactus Forage Palma. *Water* **2019**, *11*, 792. [CrossRef]
4. Teschemacher, S.; Rieger, W.; Disse, M. Experimental investigation of lateral subsurface flow depending on land use and soil cultivation. *Water* **2019**, *11*, 766. [CrossRef]
5. Fan, Y.; Clark, M.; Lawrence, D.M.; Swenson, S.; Band, L.E.; Brantley, S.L.; Brooks, P.D.; Dietrich, W.E.; Flores, A.; Grant, G.; et al. Hillslope Hydrology in Global Change Research and Earth System Modeling. *Water Resour. Res.* **2019**, *55*, 1737–1772. [CrossRef]
6. Mike, K. Hillslope runoff processes and models. *J. Hydrol.* **1988**, *100*, 315–339.
7. Kovač, Z.; Krevh, V.; Filipović, L.; Defterdarović, J.; Buškulić, P.; Han, L.; Filipović, V. Utilizing Stable Water Isotopes (Δ2H and Δ18O) To Study Soil-Water Origin in Sloped Vineyard: First Results. *Rud. Zb.* **2022**, *37*, 1–14. [CrossRef]
8. Grayson, R.B.; Western, A.W.; Chiew, F.H.S.; Blöschl, G. Preferred states in spatial soil moisture patterns: Local and nonlocal controls. *Water Resour. Res.* **1997**, *33*, 2897–2908. [CrossRef]
9. Stieglitz, M.; Shaman, J.; McNamara, J.; Engel, V.; Shanley, J.; Kling, G.W. An approach to understanding hydrologic connectivity on the hillslope and the implications for nutrient transport. *Glob. Biogeochem. Cycles* **2003**, *17*, 1105. [CrossRef]
10. McNamara, J.P.; Chandler, D.; Seyfried, M.; Achet, S. Soil moisture states, lateral flow, and streamflow generation in a semi-arid, snowmelt-driven catchment. *Hydrol. Process. Int. J.* **2005**, *19*, 4023–4038. [CrossRef]
11. Holden, J. Infiltration/Capacity/Rates. In *Water Encyclopedia*; Wiley: Hoboken, NJ, USA, 2005; pp. 212–214.
12. Mao, J.; Nierop, K.G.J.; Dekker, S.C.; Dekker, L.W.; Chen, B. Understanding the mechanisms of soil water repellency from nanoscale to ecosystem scale: A review. *J. Soils Sediments* **2019**, *19*, 171–185. [CrossRef]
13. Brendel, O. The relationship between plant growth and water consumption: A history from the classical four elements to modern stable isotopes. *Ann. For. Sci.* **2021**, *78*, 47. [CrossRef]
14. Gavrilescu, M. Water, soil, and plants interactions in a threatened environment. *Water* **2021**, *13*, 2746. [CrossRef]
15. Vereecken, H.; Weynants, M.; Javaux, M.; Pachepsky, Y.; Schaap, M.G.; van Genuchten, M.T. Using Pedotransfer Functions to Estimate the van Genuchten-Mualem Soil Hydraulic Properties: A Review. *Vadose Zone J.* **2010**, *9*, 795–820. [CrossRef]
16. Chirico, G.B.; Medina, H.; Romano, N. Functional evaluation of PTF prediction uncertainty: An application at hillslope scale. *Geoderma* **2010**, *155*, 193–202. [CrossRef]
17. Domúnguez-Niño, J.M.; Arbat, G.; Raij-Hoffman, I.; Kisekka, I.; Girona, J.; Casadesús, J. Parameterization of soil hydraulic parameters for HYDRUS-3D simulation of soil water dynamics in a drip-irrigated orchard. *Water* **2020**, *12*, 1858. [CrossRef]
18. Bezerra-Coelho, C.R.; Zhuang, L.; Barbosa, M.C.; Soto, M.A.; Van Genuchten, M.T. Further tests of the HYPROP evaporation method for estimating the unsaturated soil hydraulic properties. *J. Hydrol. Hydromech.* **2018**, *66*, 161–169. [CrossRef]

19. Lipovetsky, T.; Zhuang, L.; Teixeira, W.G.; Boyd, A.; May Pontedeiro, E.; Moriconi, L.; Alves, J.L.D.; Couto, P.; van Genuchten, M.T. HYPROP measurements of the unsaturated hydraulic properties of a carbonate rock sample. *J. Hydrol.* **2020**, *591*, 125706. [CrossRef]

20. Herbrich, M.; Gerke, H.H. Scales of Water Retention Dynamics Observed in Eroded Luvisols from an Arable Postglacial Soil Landscape. *Vadose Zone J.* **2017**, *16*, 1–17. [CrossRef]

21. Badalíková, B. Influence of Soil Tillage on Soil Compaction. In *Soil Engineering*; Springer: Berlin/Heidelberg, Germany, 2010; pp. 19–30. [CrossRef]

22. Shein, E.V.; Mady, A.Y. Hysteresis of the Water Retention Curve: Wetting Branch Simulation Based on the Drying Curve. *Mosc. Univ. Soil Sci. Bull.* **2018**, *73*, 124–128. [CrossRef]

23. Russo, D.; Jury, W.A.; Butters, G.L. Numerical analysis of solute transport during transient irrigation: 1. The effect of hysteresis and profile heterogeneity. *Water Resour. Res.* **1989**, *25*, 2109–2118. [CrossRef]

24. Weihermüller, L.; Lehmann, P.; Herbst, M.; Rahmati, M.; Verhoef, A.; Or, D.; Jacques, D.; Vereecken, H. Choice of Pedotransfer Functions Matters when Simulating Soil Water Balance Fluxes. *J. Adv. Model. Earth Syst.* **2021**, *13*, e2020MS002404. [CrossRef]

25. Van Looy, K.; Bouma, J.; Herbst, M.; Koestel, J.; Minasny, B.; Mishra, U.; Montzka, C.; Nemes, A.; Pachepsky, Y.A.; Padarian, J.; et al. Pedotransfer Functions in Earth System Science: Challenges and Perspectives. *Rev. Geophys.* **2017**, *55*, 1199–1256. [CrossRef]

26. Rodríguez, A.; Ruiz-Ramos, M.; Palosuo, T.; Carter, T.R.; Fronzek, S.; Lorite, I.J.; Ferrise, R.; Pirttioja, N.; Bindi, M.; Baranowski, P.; et al. Implications of crop model ensemble size and composition for estimates of adaptation effects and agreement of recommendations. *Agric. For. Meteorol.* **2019**, *264*, 351–362. [CrossRef] [PubMed]

27. Dion, P.; Martel, J.L.; Arsenault, R. Hydrological ensemble forecasting using a multi-model framework. *J. Hydrol.* **2021**, *600*, 126537. [CrossRef]

28. Riggers, C.; Poeplau, C.; Don, A.; Bamminger, C.; Höper, H.; Dechow, R. Multi-model ensemble improved the prediction of trends in soil organic carbon stocks in German croplands. *Geoderma* **2019**, *345*, 17–30. [CrossRef]

29. Tebaldi, C.; Knutti, R. The use of the multi-model ensemble in probabilistic climate projections. *Philos. Trans. R. Soc. A Math. Phys. Eng. Sci.* **2007**, *365*, 2053–2075. [CrossRef]

30. Filipović, V.; Defterdarović, J.; Krevh, V.; Filipović, L.; Ondrašek, G.; Kranjčec, F.; Magdić, I.; Rubinić, V.; Stipičević, S.; Mustać, I.; et al. Estimation of stagnosol hydraulic properties and water flow using uni-and bimodal porosity models in erosion-affected hillslope vineyard soils. *Agronomy* **2022**, *12*, 33. [CrossRef]

31. Pütz, T.; Kiese, R.; Wollschläger, U.; Groh, J.; Rupp, H.; Zacharias, S.; Priesack, E.; Gerke, H.H.; Gasche, R.; Bens, O.; et al. TERENO-SOILCan: A lysimeter-network in Germany observing soil processes and plant diversity influenced by climate change. *Environ. Earth Sci.* **2016**, *75*, 1242. [CrossRef]

32. Groh, J.; Slawitsch, V.; Herndl, M.; Graf, A.; Vereecken, H.; Pütz, T. Determining dew and hoar frost formation for a low mountain range and alpine grassland site by weighable lysimeter. *J. Hydrol.* **2018**, *563*, 372–381. [CrossRef]

33. Peters, A.; Nehls, T.; Schonsky, H.; Wessolek, G. Separating precipitation and evapotranspiration from noise—A new filter routine for high-resolution lysimeter data. *Hydrol. Earth Syst. Sci.* **2014**, *18*, 1189–1198. [CrossRef]

34. Peters, A.; Nehls, T.; Wessolek, G. Technical note: Improving the AWAT filter with interpolation schemes for advanced processing of high resolution data. *Hydrol. Earth Syst. Sci.* **2016**, *20*, 2309–2315. [CrossRef]

35. Peters, A.; Groh, J.; Schrader, F.; Durner, W.; Vereecken, H.; Pütz, T. Towards an unbiased filter routine to determine precipitation and evapotranspiration from high precision lysimeter measurements. *J. Hydrol.* **2017**, *549*, 731–740. [CrossRef]

36. Lazarević, B.; Šatović, Z.; Nimac, A.; Vidak, M.; Gunjača, J.; Politeo, O.; Carović-Stanko, K. Application of Phenotyping Methods in Detection of Drought and Salinity Stress in Basil (*Ocimum basilicum* L.). *Front. Plant Sci.* **2021**, *12*, 629441. [CrossRef] [PubMed]

37. Carsel, R.F.; Parrish, R.S. Developing Joint Probability Distributions of Soil Water Retention Characteristics. *Water Resour. Res.* **1988**, *24*, 755–769. [CrossRef]

38. Schaap, M.G.; Leij, F.J.; van Genuchten, M.T. Rosetta: A computer program for estimating soil hydraulic parameters with hierarchical pedotransfer functions. *J. Hydrol.* **2001**, *251*, 163–176. [CrossRef]

39. Wösten, J.H.M.; Lilly, A.; Nemes, A.; Le Bas, C. Development and use of a database of hydraulic properties of European soils. *Geoderma* **1999**, *90*, 169–185. [CrossRef]

40. Rawls, W.J.; Braksiek, D.L. Prediction of Soil Water Properties for Hydrologic Modelling. In *Watershed Management in the Eighties, Proceedings of the Symposium Sponsored by the Committee on Watershed Management of the Irrigation and Drainage Division of the American Society of Civil Engineers in Conjunction with the ASCE Convention, Denver, CO, USA, 30 April–1 May 1985*; Jones, E.B., Ward, T.J., Eds.; ASCE: New York, NY, USA, 1985; pp. 293–299.

41. Weynants, M.; Vereecken, H.; Javaux, M. Revisiting Vereecken Pedotransfer Functions: Introducing a Closed-Form Hydraulic Model. *Vadose Zone J.* **2009**, *8*, 86–95. [CrossRef]

42. Tóth, B.; Weynants, M.; Nemes, A.; Makó, A.; Bilas, G.; Tóth, G. New generation of hydraulic pedotransfer functions for Europe. *Eur. J. Soil Sci.* **2015**, *66*, 226–238. [CrossRef]

43. Campbell, G.; Campbell, C.; Cobos, D.; Crawford, L.B.; Rivera, L.; Chambers, C. *Operation Manual HYPROP*; UMS: Munich, Germany, 2015; pp. 1–95.

44. *METER WP4C Manual*; Meter: Pullman, WA, USA, 2021; pp. 1–40.

45. Vrugt, J.A.; Gupta, H.V.; Bouten, W.; Sorooshian, S. A Shuffled Complex Evolution Metropolis algorithm for optimization and uncertainty assessment of hydrologic model parameters. *Water Resour. Res.* **2003**, *39*, 1201. [CrossRef]

46. Ries, F.; Lange, J.; Schmidt, S.; Puhlmann, H.; Sauter, M. Recharge estimation and soil moisture dynamics in a Mediterranean, semi-arid karst region. *Hydrol. Earth Syst. Sci.* **2015**, *19*, 1439–1456. [CrossRef]

47. Groh, J.; Stumpp, C.; Lücke, A.; Pütz, T.; Vanderborght, J.; Vereecken, H. Inverse Estimation of Soil Hydraulic and Transport Parameters of Layered Soils from Water Stable Isotope and Lysimeter Data. *Vadose Zone J.* **2018**, *17*, 1–19. [CrossRef]

48. Šimůnek, J.; van Genuchten, M.T.; Šejna, M. Recent Developments and Applications of the HYDRUS Computer Software Packages. *Vadose Zone J.* **2016**, *15*, vzj2016.04.0033. [CrossRef]

49. Van Genuchten, M.T. A closed-form equation for predicting the hydraulic conductivity of unsaturated soils. *Soil Sci. Soc. Am. J.* **1980**, *44*, 892–898. [CrossRef]

50. Allen, R.G.; Pruitt, W.O.; Wright, J.L.; Howell, T.A.; Ventura, F.; Snyder, R.; Itenfisu, D.; Steduto, P.; Berengena, J.; Yrisarry, J.B.; et al. A recommendation on standardized surface resistance for hourly calculation of reference ETo by the FAO56 Penman-Monteith method. *Agric. Water Manag.* **2006**, *81*, 1–22. [CrossRef]

51. Allen, R.G.; Pereira, L.S.; Raes, D.; Smith, M. FAO Irrigation and Drainage Paper No. 56—Crop Evapotranspiration. In *Crop Evapotranspiration. Guidelines for Computing Crop Water Requirements*; Food and Agriculture Organization: Rome, Italy, 1998.

52. Kanso, T.; Tedoldi, D.; Gromaire, M.C.; Ramier, D.; Saad, M.; Chebbo, G. Horizontal and vertical variability of soil hydraulic properties in roadside sustainable drainage systems (SuDS)-nature and implications for hydrological performance evaluation. *Water* **2018**, *10*, 987. [CrossRef]

53. Kool, D.; Tong, B.; Tian, Z.; Heitman, J.L.; Sauer, T.J.; Horton, R. Soil water retention and hydraulic conductivity dynamics following tillage. *Soil Tillage Res.* **2019**, *193*, 95–100. [CrossRef]

54. Assouline, S. Infiltration into soils: Conceptual approaches and solutions. *Water Resour. Res.* **2013**, *49*, 1755–1772. [CrossRef]

55. Yang, Y.; Chen, R.S.; Song, Y.X.; Han, C.T.; Liu, Z.W.; Liu, J.F. Spatial variability of soil hydraulic conductivity and runoff generation types in a small mountainous catchment. *J. Mt. Sci.* **2020**, *17*, 2724–2741. [CrossRef]

56. Vereecken, H.; Schnepf, A.; Hopmans, J.W.; Javaux, M.; Or, D.; Roose, T.; Vanderborght, J.; Young, M.H.; Amelung, W.; Aitkenhead, M.; et al. Modeling Soil Processes: Review, Key Challenges, and New Perspectives. *Vadose Zone J.* **2016**, *15*, vzj2015.09.0131. [CrossRef]

57. Groh, J.; Diamantopolous, E.; Duan, X.; Ewert, F.; Herbst, M.; Holbak, M.; Kamali, B.; Kersebaum, K.-C.; Kuhnert, M.; Lischeid, G.; et al. Crop growth and soil water fluxes at erosion-affected arable sites; Using weighing lysimeter data for model intercomparison. *Vadose Zone J.* **2020**, *19*, e20058. [CrossRef]

58. Šimůnek, J.; Jarvis, N.J.; van Genuchten, M.T.; Gärdenäs, A. Review and comparison of models for describing non-equilibrium and preferential flow and transport in the vadose zone. *J. Hydrol.* **2003**, *272*, 14–35. [CrossRef]

59. Cloke, H.L.; Renaud, J.P.; Claxton, A.J.; McDonnell, J.J.; Anderson, M.G.; Blake, J.R.; Bates, P.D. The effect of model configuration on modelled hillslope-riparian interactions. *J. Hydrol.* **2003**, *279*, 167–181. [CrossRef]

60. Dekker, L.W.; Ritsema, C.J. How water moves in a water repellent sandy soil: 1. Potential and actual water repellency. *Water Resour. Res.* **1994**, *30*, 2507–2517. [CrossRef]

61. Dymond, S.F.; Wagenbrenner, J.W.; Keppeler, E.T.; Bladon, K.D. Dynamic Hillslope Soil Moisture in a Mediterranean Montane Watershed. *Water Resour. Res.* **2021**, *57*, e2020WR029170. [CrossRef]

62. Islam, N.; Wallender, W.W.; Mitchell, J.P.; Wicks, S.; Howitt, R.E. Performance evaluation of methods for the estimation of soil hydraulic parameters and their suitability in a hydrologic model. *Geoderma* **2006**, *134*, 135–151. [CrossRef]

63. Gijsman, A.; Jagtap, S.; Jones, J. Wading through a swamp of complete confusion: How to choose a method for estimating soil water retention parameters for crop models. *Eur. J. Agron.* **2002**, *18*, 77–106. [CrossRef]

64. Baroni, G.; Facchi, A.; Gandolfi, C.; Ortuani, B.; Horeschi, D.; van Dam, J.C. Uncertainty in the determination of soil hydraulic parameters and its influence on the performance of two hydrological models of different complexity. *Hydrol. Earth Syst. Sci.* **2010**, *14*, 251–270. [CrossRef]